

# Investigation of ground-state properties of even-even and odd Pb isotopes within Hartree-Fock-Bogoliubov theory

**Y. EL BASSEM<sup>1</sup>, M. OULNE<sup>1</sup>**

<sup>1</sup>High Energy Physics and Astrophysics Laboratory, Department of Physics,  
Faculty of Sciences SEMLALIA, Cadi Ayyad University,  
P.O.B. 2390, Marrakesh, Morocco.

**Abstract.** The nuclear structure of even-even and odd lead isotopes ( $^{178-236}\text{Pb}$ ) is investigated within the Hartree-Fock-Bogoliubov theory. Calculations are performed for a wide range of neutron numbers, starting from the proton-rich side up to the neutron-rich side, by using the SLy4 Skyrme interaction and a new proposed formula for the pairing strength which is more precise for this region of nuclei as we did in previous works in the regions of Neodymium (Nd,  $Z=60$ ) [Int. J. Mod. Phys. E 24, 1550073 (2015)] and Molybdenum (Mo,  $Z=42$ ) [Nuc. Phys. A 957 22-32 (2017)]. Such a new pairing strength formula allows reaching exotic nuclei region where the experimental data are not available. Calculated values of various physical quantities such as binding energy, two-neutron separation energy, and rms-radii for protons and neutrons are discussed and compared with experimental data and some estimates of other nuclear models like Finite Range Droplet Model (FRDM), Relativistic Mean Field (RMF), Density-Dependent Meson-Exchange Relativistic Energy Functional (DD-ME2) and results of Hartree-Fock-Bogoliubov calculations based on the DIS Gogny effective nucleon-nucleon interaction (Gogny DIS).

## 1 Introduction

A long-standing goal of research in nuclear physics is to make reliable predictions with one nuclear model in order to describe the ground-state properties of all nuclei in the nucleic chart. For this purpose, several approaches have been developed to study ground-state and single-particle (s.p) excited states properties of nuclei. For Light nuclei with a mass number up to  $A \approx 12$ , *ab initio* calculations employing the realistic nucleon-nucleon and three-nucleon interactions with the Green's function Monte Carlo (GFMC) method are applicable [1]. While these methods have been successful in the case of light nuclei, their applications to heavier systems become rather difficult due to the numerical difficulties in handling the nuclear many-body problem. For medium-mass nuclei up to  $A \approx 60$ , the large-scale shell model [2] may be used. While for heavier nuclei, non-relativistic [3–7] and relativistic [8,9] mean field theories have received

much attention for describing the ground-state properties of nuclei. One of the most important phenomenological approaches widely used in nuclear structure calculations is the Hartree-Fock-Bogoliubov method [10], which allows particles and holes to be treated on an equal footing by unifying the self-consistent description of nuclear orbitals, as given by Hartree-Fock (HF) approach, and the Bardeen-Cooper-Schrieffer (BCS) pairing theory [11] into a single variational method.

The region of lead (Pb) is very important for studying the nuclear structure, since  $Z = 82$  is a typical proton magic number. Plenty of experimental data and many theoretical models have been employed to investigate the nuclei in this region [12]. In the present work, we intend to check the validity of our treatment on the structure and properties of lead isotopes. In this treatment we will use the HFB method with SLy4 Skyrme interaction [5] and a new proposed formula for the pairing strength.

The paper is organized as follows. In Section 2, a brief review of the Hartree-Fock-bogoliubov method is provided. Details about the numerical calculations are presented in Section 3. While Section 4 is devoted to present our results and discussion. A summary of the present study is given in Section 5.

## 2 Hartree-Fock-Bogoliubov Method

The Hartree-Fock-Bogoliubov (HFB) [13, 14] method with effective zero-range pairing forces is a reliable and computational convenient way to study the nuclear pairing correlations in both stable and unstable nuclei. The HFB framework has been extensively discussed in the literature [13, 15–17] and will be briefly introduced here.

In the standard HFB method, a two-body Hamiltonian of a system of fermions can be expressed in terms of a set of annihilation and creation operators ( $c, c^\dagger$ ):

$$H = \sum_{n_1 n_2} e_{n_1 n_2} c_{n_1}^\dagger c_{n_2} + \frac{1}{4} \sum_{n_1 n_2 n_3 n_4} \bar{v}_{n_1 n_2 n_3 n_4} c_{n_1}^\dagger c_{n_2}^\dagger c_{n_4} c_{n_3} \quad (1)$$

with the first term corresponding to the kinetic energy and  $\bar{v}_{n_1 n_2 n_3 n_4} = \langle n_1 n_2 | V | n_3 n_4 - n_4 n_3 \rangle$  are anti-symmetrized two-body interaction matrix-elements. In HFB method, the ground-state wave function  $|\Phi\rangle$  is defined as the quasi-particle vacuum  $\alpha_k |\Phi\rangle = 0$ , in which the quasi-particle operators ( $\alpha, \alpha^\dagger$ ) are connected to the original particle ones via a linear Bogoliubov transformation:

$$\alpha_k = \sum_n (U_{nk}^* c_n + V_{nk}^* c_n^\dagger), \quad \alpha_k^\dagger = \sum_n (V_{nk} c_n + U_{nk} c_n^\dagger), \quad (2)$$

which can be rewritten in the matrix form as:

$$\begin{pmatrix} \alpha \\ \alpha^\dagger \end{pmatrix} = \begin{pmatrix} U^\dagger & V^\dagger \\ V^T & U^T \end{pmatrix} \begin{pmatrix} c \\ c^\dagger \end{pmatrix}, \quad (3)$$

The matrices  $U$  and  $V$  satisfy the relations:

$$\begin{aligned} U^\dagger U + V^\dagger V &= 1, & UU^\dagger + V^*V^T &= 1, \\ U^T V + V^T U &= 0, & UV^\dagger + V^*U^T &= 0. \end{aligned} \quad (4)$$

The basic building blocks of this theory are the density matrix and the pairing tensor. In terms of the normal  $\rho$  and pairing  $\kappa$  one-body density matrices, defined as:

$$\begin{aligned} \rho_{nn'} &= \langle \Phi | c_{n'}^\dagger c_n | \Phi \rangle = (V^*V^T)_{nn'}, \\ \kappa_{nn'} &= \langle \Phi | c_{n'} c_n | \Phi \rangle = (V^*U^T)_{nn'}, \end{aligned} \quad (5)$$

the expectation value of the Hamiltonian (1) is expressed as an energy functional

$$E[\rho, \kappa] = \frac{\langle \Phi | H | \Phi \rangle}{\langle \Phi | \Phi \rangle} = \text{Tr}[(e + \frac{1}{2}\Gamma)\rho] - \frac{1}{2}\text{Tr}[\Delta\kappa^*] \quad (6)$$

where

$$\begin{aligned} \Gamma_{n_1 n_3} &= \sum_{n_2 n_4} \bar{v}_{n_1 n_2 n_3 n_4} \rho_{n_4 n_2} \\ \Delta_{n_1 n_2} &= \frac{1}{2} \sum_{n_3 n_4} \bar{v}_{n_1 n_2 n_3 n_4} \kappa_{n_3 n_4}. \end{aligned} \quad (7)$$

The variation of the energy (6) with respect to  $\rho$  and  $\kappa$  leads to the HFB equations:

$$\begin{pmatrix} e + \Gamma - \lambda & \Delta \\ -\Delta^* & -(e + \Gamma)^* + \lambda \end{pmatrix} \begin{pmatrix} U \\ V \end{pmatrix} = E \begin{pmatrix} U \\ V \end{pmatrix}, \quad (8)$$

where  $\Delta$  and  $\lambda$  denote the pairing potential and Lagrange multiplier, introduced to fix the correct average particle number, respectively.

It should be stressed that the energy functional (6) contains terms that cannot be simply related to some prescribed effective interaction [17]. In terms of Skyrme forces, the HFB energy (6) has the form of local energy density functional:

$$E[\rho, \tilde{\rho}] = \int d^3\mathbf{r} \mathbf{H}(\mathbf{r}), \quad (9)$$

where  $\mathbf{H}(\mathbf{r})$  is the sum of the mean field and pairing energy densities.

$$\mathbf{H}(\mathbf{r}) = H(\mathbf{r}) + \tilde{H}(\mathbf{r}) \quad (10)$$

We use the pairing density matrix  $\tilde{\rho}$ ,

$$\tilde{\rho}(\mathbf{r}\sigma, \mathbf{r}'\sigma') = -2\sigma'\kappa(\mathbf{r}, \sigma, \mathbf{r}', -\sigma') \quad (11)$$

instead of the pairing tensor  $\kappa$ . This is convenient for describing time-even quasiparticle states when both  $\rho$  and  $\tilde{\rho}$  are hermitian and time-even [15].

The variation of the energy (9) with respect to the particle local density  $\rho$  and pairing local density  $\tilde{\rho}$  results in the Skyrme HFB equations:

$$\sum_{\sigma'} \begin{pmatrix} h(\mathbf{r}, \sigma, \sigma') & \Delta(\mathbf{r}, \sigma, \sigma') \\ \Delta(\mathbf{r}, \sigma, \sigma') & -h(\mathbf{r}, \sigma, \sigma') \end{pmatrix} \begin{pmatrix} U(E, \mathbf{r}\sigma') \\ V(E, \mathbf{r}\sigma') \end{pmatrix} = \begin{pmatrix} E + \lambda & 0 \\ 0 & E - \lambda \end{pmatrix} \begin{pmatrix} U(E, \mathbf{r}\sigma) \\ V(E, \mathbf{r}\sigma) \end{pmatrix} \quad (12)$$

where  $\lambda$  is the chemical potential. The local fields  $h(\mathbf{r}, \sigma, \sigma')$  and  $\Delta(\mathbf{r}, \sigma, \sigma')$  can be calculated in coordinate space. Details can be found in Refs. [13, 18, 19].

### 3 Details of Calculations

In this work, the ground-state properties of even-even and odd  $^{178-236}\text{Pb}$  have been reproduced by using the computer code HFBTHO (v2.00d) [20] which utilizes the axial Transformed Harmonic Oscillator (THO) single-particle basis to expand quasi-particle wave functions. It iteratively diagonalizes the Hartree-Fock-Bogoliubov Hamiltonian based on generalized Skyrme-like energy densities and zero-range pairing interactions until a self-consistent solution is found.

Calculations were performed with the SLy4 Skyrme functional [15] as in Ref. [18], and by using the same parameters as in our previous works [21, 22]: A quasi-particle cutoff of  $E_{cut} = 60 \text{ MeV}$ , which means that only quasi-particle states with energy lower than  $60 \text{ MeV}$  are taken into account, and a mixed surface-volume pairing with identical pairing strength for both protons and neutrons. The number of oscillator shells taken into account was  $N_{max} = 20 \text{ shells}$ , the total number of states in the basis  $N_{states} = 500$ , and the value of the deformation  $\beta$  is taken from the column  $\beta_2$  of the Ref. [23]. The THO basis is characterized by the frequency  $\hbar\omega_0 = 1.2*41/A^{1/3}$ , and the length  $b_0$  is automatically sets by using the relation  $b_0 = \sqrt{\hbar/m\omega_0}$ . The number of Gauss-Laguerre and Gauss-Hermite quadrature points was  $N_{GL} = N_{GH} = 40$ , and the number of Gauss-Legendre points for the integration of the Coulomb potential was  $N_{Leg} = 80$  [21, 22].

Odd-N isotopes are calculated by using the blocking of quasi-particle states [24]. The time-reversal symmetry is, by construction, conserved in the computer code HFBTHO (v2.00d), the blocking prescription is implemented in the equal filling approximation [24, 25], and the time-odd fields of the Skyrme functional are identically zero. The identification of the blocking candidate is done using the same technique as in HFODD [26]: the mean-field Hamiltonian  $h$  is diagonalized at each iteration and provides a set of equivalent single-particle states. Based on the Nilsson quantum numbers of the requested blocked level provided in the input file, the code identifies the index of the quasi-particle (q.p.) to be

blocked by looking at the overlap between the q.p. wave-function (both lower and upper component separately) and the s.p. wave-function. The maximum overlap specifies the index of the blocked q.p. [20].

In the present work, among several parameters sets for prediction of the nuclear ground state properties [27,28], we used the SLy4 Skyrme force [15] which is widely used in nuclear structure calculations.

As in Refs. [21,22], in the input data file of the computer code HFBTHO (v2.00d) [20], we have modified the values of the pairing strength for neutrons  $V_0^n$  and protons  $V_0^p$  (in MeV), which may be different, but in our study the pairing strength  $V_0^{n,p}$  is taken to be the same for both. At each time, we have executed the code and compared the obtained ground-state total binding energy with the experimental value. This procedure was repeated until we found the value of  $V_0^{n,p}$  that gives the ground-state total binding energy closest to the experimental one. For more details, see Refs. [21,22] and references therein.

By fitting the obtained values of  $V_0^{n,p}$  to the mass number  $A$ , we have found the following formula:

$$V_0^{n,p} = 7.28 A^{\frac{3}{4}} \quad (13)$$

In order to check the validity of Eq. (13), it has been used to generate the pairing-strength  $V_0^{n,p}$  for each mass number  $A$ , then we have included this value of  $V_0^{n,p}$  in the input data file of the computer code HFBTHO (v2.00d) so as to calculate several ground-state properties such as binding energy, two-neutron separation energy, charge, neutron and proton radii. The obtained results are presented in the next section.

## 4 Results and Discussion

In this section we present the numerical results of this work, particularly for binding energy, two-neutron separation energy, charge, neutron and proton radii for  $^{178-236}\text{Pb}$  isotopes.

In all our calculations, we used the Skyrme force (SLy4) and Eq. (13) for the pairing strength.

### 4.1 Binding energy

Binding Energy (BE) is a very important quantity in nuclear physics and one of the key observables for understanding the structure of a nucleus. The calculated Binding Energies per nucleon (BE/A) for lead isotopes, obtained by using the pairing strength generated by Eq. (13) and those obtained by direct calculation (by using the default value of the pairing strength "Direct Calc.") are plotted in Fig. 1 as function of the neutron number  $N$ . The experimental binding energies per nucleon [29], as well as the HFB calculations based on the D1S Gogny force [30]. The predictions of the Finite Range Droplet Model (FRDM) [31], the Relativistic Mean Field (RMF) model with NL3 functional [9], and the Density-

Dependent Meson-Exchange Relativistic Energy Functional (DD-ME2) [32] are also shown in Fig. 1 for comparison.

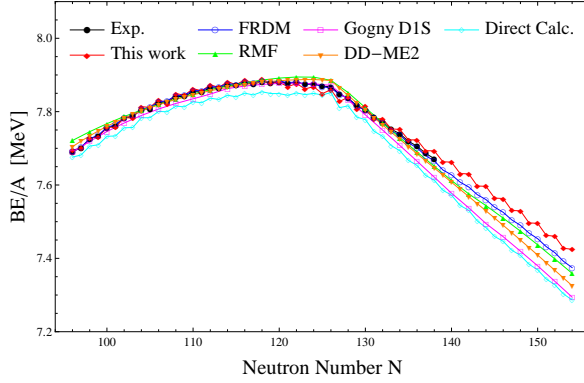


Figure 1. (Color online) Binding energies per nucleon for even-even and odd *Pb* isotopes.

From Fig. 1, it is seen that the binding energies per particle for *Pb* isotopes produced by our calculations using HFB with SLy4 parameter set, are in a good agreement with the experimental data. We note that the maximum in the binding energy per nuclei, (BE/A), for lead isotopes is observed at the magic neutron number  $N = 126$ .

In order to provide a further check of the accuracy of our results, the differences between the experimental total BE and the calculated results obtained in this work by using Eq. (13) are shown as function of the neutron number  $N$  in Fig. 2. The results of other nuclear models are also included for comparison. We point out that this comparison is made only for isotopes that have available experimental data.

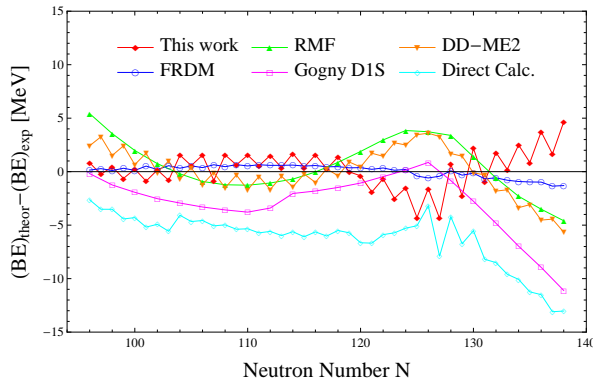


Figure 2. (Color online) Differences between calculated results for total binding energies and experimental values.

The root-mean-square (rms) deviation between the calculated results in the present study and the experimental data are listed in Table 1. The predictions of FRDM [31] and RMF [9] theories as well as the HFB calculations based on the D1S Gogny force [30] are listed too for comparison.

Table 1. The rms deviation  $(BE/A)_{theor} - (BE/A)_{exp}$  (in MeV).

This work	Direct Calc.	RMF	FRDM	Gogny D1S	DD-ME2
0.0086	0.0325	0.0130	0.0028	0.0193	0.0105

As we can see from Table 1, our work exceeds in accuracy all the other nuclear models, except the FRDM which is the most accurate.

## 4.2 Neutron separation energy

The two-neutron separation energy,  $S_{2n}$ , is an important quantity in investigating the nuclear shell structure and in testing the validity of a model. In the present work, we calculated the two-neutron separation energies for lead isotopes in SLy4 parametrization with the pairing strength  $V_0^{n,p}$  generated by Eq. (13). The double neutron separation energy is defined as:

$$S_{2n}(Z, N) = BE(Z, N) - BE(Z, N - 2) \quad (14)$$

Note that in using this equation, all binding energies must be entered with a positive sign. The calculated  $S_{2n}$  for lead isotopes are displayed in Fig. 3. The available experimental data [29], and the predictions of other nuclear models such as RMF [9], FRDM [31], Gogny D1S [30] and DD-ME2 [32] are also presented for comparison.

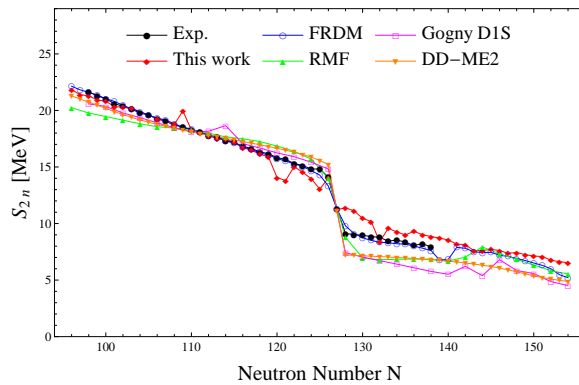


Figure 3. (Color online) The double neutron separation energy,  $S_{2n}$ , of Pb isotopes.

As one can see from Fig. 3, the two-neutron separation energies are getting smaller and smaller as the neutron number  $N$  increases. Also, a sharp decline is clearly seen at  $N = 126$  both in the experimental and theoretical curves, which indicates the closed shell at this magic neutron number. Moreover, except for few lead isotopes, our calculated values are in a good agreement with the experimental data and have the lowest rms deviation in comparison with the results of RMF, Gogny D1S and DD-ME2, as we can see from Table 2.

Table 2. The rms deviation  $(S_{2n})_{theor} - (S_{2n})_{exp}$  (in Mev).

This work	RMF	FRDM	Gogny D1S	DD-ME2
0.9679	1.1343	0.2394	1.1948	0.9847

### 4.3 Neutron, Proton and Charge radii

The root-mean-square (rms) charge radius,  $R_c$ , is related to the rms proton radius,  $R_p$ , by :

$$R_c^2 = R_p^2 + 0.64 (fm^2) \quad (15)$$

where the factor 0.64 in Eq. (15) accounts for the finite-size effects of the proton. Fig. 4 shows the rms charge radii of lead isotopes calculated in this work. For the sake of comparison, it also shows the available experimental data [33] and the predictions of other nuclear models.

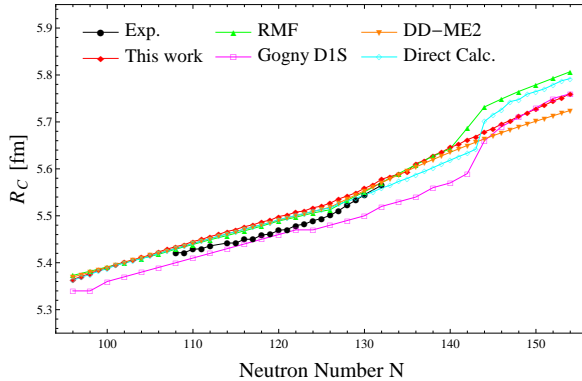


Figure 4. (Color online) The charge radii of  $Pb$  isotopes.

From Fig. 4, a rather good agreement between theory and experiment can be clearly seen. The root-mean-square (rms) deviation between our calculated charge radii and their experimental counterparts is less than 0.024 fm as well as in the case of HFB calculations based on the D1S Gogny force [30], and it did not exceed 0.018 fm for the other models.



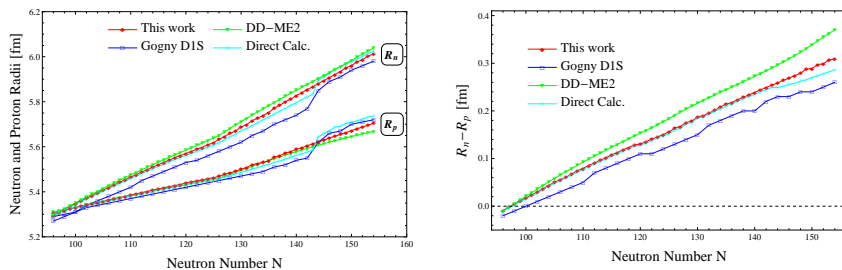


Figure 5. (Color online) The neutron and proton radii (left panel) and the neutron skin thicknesses ( $\Delta R = R_n - R_p$ ) (right panel) of *Pb* isotopes.

Fig. 5 (left panel) shows both the neutron and proton radii ( $R_n$  and  $R_p$ ) of lead isotopes obtained in our calculations as function of the neutron number  $N$ . The HFB calculations based on the D1S Gogny force [30] are shown for comparison as well as the results of the relativistic Hartree-Bogoliubov (RHB) model with the DD-ME2 effective interaction that we have calculated by using the computer code DIRHBZ [34]. The difference between  $R_n$  and  $R_p$  ( $\Delta R = R_n - R_p$ ), i.e. neutron skin is also shown in Fig. 5 (right panel).

As it can be seen from Fig. 5, In the vicinity of the  $\beta$ -stability line ( $N \approx Z$ ), the neutron and proton radii are approximately the same. The difference between  $R_n$  and  $R_p$  ( $\Delta R = R_n - R_p$ ) increases monotonously with increasing the neutron number, in favor of developing a neutron skin.  $\Delta R$  attains its maximum for  $^{236}\text{Pb}$ , in which it reaches 0.308 fm in our calculation, and 0.370 fm and 0.260 fm in DD-ME2 and Gogny D1S nuclear models, respectively.

## 5 Conclusion

In the present work, we have studied the ground-state properties of even and odd lead isotopic chain,  $^{178-236}\text{Pb}$ , from the proton drip line to the neutron drip line in the framework of HFB theory with SLy4 Skyrme force. The calculations were made by using the computer code HFBTHO (v2.00d), in which the pairing strength was given by our new generalized formula that gives, for each mass number  $A$ , the appropriate pairing strength  $V_0^{n,p}$  for neutrons and protons instead of the default value which is constant whatever the mass number. Our calculations reproduce the available experimental data very well including the nuclear binding energies, two-neutron separation energies. The parabolic behavior of the  $BE/A$  has been well reproduced in respect to the experimental curve. The calculated charge radii are also coherent with the experimental data for most nuclei. The neutron skin, in our calculation, reaches 0.308 for  $^{236}\text{Pb}$ .

## References

- [1] P. Navratil, B.R. Barrett, W.E. Ormand, Phys. Rev C 56 (1997) 2542.

- [2] S.E. Koonin, D.J. Dean, K. Langanke, Phys. Rep. 1 (1997) 278.
- [3] J. Terasaki, P.H. Heenen, H. Flocard, P. Bonche, Nucl. Phys. A 600 (1996) 371-386.
- [4] M.V. Stoitsov, *et al.*, Phys. Rev. C - Nucl. Phys. 61 (2000) 034311.
- [5] E. Chabanat, *et al.*, Nucl. Phys. A 635 (1998) 231-256.
- [6] E. Terán, V.E. Oberacker, A.S. Umar, Phys. Rev. C 67 (2003) 064314.
- [7] J. Dobaczewski, *et al.*, Phys. Rev. C 53 (1996) 2809.
- [8] P. Ring, Prog. Part. Nucl. Phys. 37 (1996) 193-263.
- [9] G.A. Lalazissis, S. Raman, P. Ring, *Atom. Data Nucl. Data Tables* 71 (1999) 1-40.
- [10] M. Yamagami, K. Matsuyanagi, M. Matsuo, Nucl. Phys. A 693 (2001) 579-602.
- [11] J. Bardeen, L.N. Cooper, J.R. Schrieffer, Phys. Rev. 108 (1957) 1175.
- [12] R. Julin, K. Helariutta, M. Muikki, J. Phys. G 27 (2001) R109.
- [13] P. Ring, P. Schuck, *et al.*, (New York, Springer-Verlag, 1980).
- [14] N.N. Bogoliubov, Sov. Phys. Usp. 673 (1959) 236.
- [15] J. Dobaczewski, H. Flocard, and J. Treiner, Nucl. Phys. A, 422 (1984) 103-139.
- [16] J. Dobaczewski *et al.*, Phys. Rev. C 53 (1996) 2809.
- [17] M. Bender, P.H. Heenen, P.G. Reinhard, Rev. Mod. Phys. 75 (2003) 121.
- [18] M.V. Stoitsov, *et al.*, 167 (2005) 43-63.
- [19] W. Greiner, J.A. Maruhn, Berlin, Springer-Verlag, (1995).
- [20] M.V. Stoitsov, *et al.*, Comp. Phys. Commun. 184 (2013) 1592-1604.
- [21] Y. EL Bassem, M. Oulne, Int. J. Mod. Phys. E 24 (2015) 1550073.
- [22] Y. EL Bassem, M. Oulne, Nucl. Phys. A 957 (2017) 22-32.
- [23] P. Moller, *et al.*, Atomic Data and Nuclear Data Tables, 59 (1995) 185-381.
- [24] N. Schunck, *et al.*, Phys. Rev. C 81 (2010) 024316.
- [25] S. Perez-Martin, L.M. Robledo, Phys. Rev. C, 78 (2008) 014304.
- [26] J. Dobaczewski *et al.*, Computer Physics Communications 180 (2009) 2361-2391.
- [27] J. Bartel *et al.*, Nucl. Phys. A 386 (1982) 79-100.
- [28] A. Baran, *et al.*, J. Phys. G. 21 (1995) 657.
- [29] M. Wang *et al.* Chinese Physics C, 36 (2012) 1603.
- [30] S. Hilaire, M. Girod, Eur. Phys. J. A, 33.2 (2007) 237-241.
- [31] P.Möller, *et al.*, *Data Nucl. Data Tables* 66 (1997) 131-343.
- [32] G.A. Lalazissis, *et al.*, Phys. Rev. C 71 (2005) 024312.
- [33] I. Angeli. *Atomic data and nuclear data tables*, 87 (2004) 185-206.
- [34] T. Nikšić *et al.*, Computer Physics Communications 185 (2014) 1808-1821.